Reequilibration of fluid inclusions in garnet and kyanite from metapelites of the Radenthein Complex, Austroalpine Basement, Austria

Autor(en): **Kaindl, Reinhard / Abart, Reiner**

Reequilibration of fluid inclusions in garnet and kyanite from metapelites of the Radenthein Complex, Austroalpine Basement, Austria

by *Reinhard Kaindl[1]* and *Rainer Abart[1]*

Abstract

Amphibolite facies metapelites of the Radenthein Complex from the Austroalpine basement contain texturally primary fluid inclusions in the metamorphic index minerals garnet and kyanite and in quartz. Geothermobarometry, stable isotope data and fluid inclusion studies revealed discrepancies between peak metamorphic conditions on the one hand and observed fluid compositions and densities of the primary fluid on the other hand. Oxygen isotope thermometry on several mineral pairs yielded concordant peak metamorphic temperatures in the range of 560 to 590 °C. Combination of these temperature estimates with the analysis of phase relations suggests peak pressures between 5.5 and 7.5 kilobars and the presence of a mixed-volatile pore fluid with a water content of X_{H_2O} between 0.4 and 0.5 and with a molar volume of about 31 cm^3/mol. The garnet- and kyanite-hosted primary fluid inclusions belong to the CO_2–N_2, and CO_2–H_2O systems, respectively. The generally low X_{H_2O} (< 0.26) of the fluid and the high fluid molar volumes of 45 to 74 cm^3/mol are inconsistent with the estimated peak metamorphic conditions indicating post-entrapment modifications of the primary fluid inclusions. We suggest that two mechanisms, the loss of H_2O due to pressure or fugacity gradients from the inclusions to the pore fluid and the selective removal of H_2O in the course of chemical reaction between the inclusion fluid and the respective host mineral were responsible for these modifications. The latter mechanism is corroborated by the presence of chlorite aggregates within the primary inclusions, which are interpreted as the products of retrograde hydration reactions between a water-bearing inclusion fluid and the garnet host. Theoretical considerations are presented which confirm that a combination of both reequilibration mechanisms can fully explain the discrepancies between the inferred peak metamorphic conditions and the observed fluid compositions and densities.

Keywords: Metapelites, fluid inclusions, geothermobarometry, post-entrapment effects, retrograde reactions.

Introduction

Fluid inclusions provide a unique possibility to directly observe metamorphic fluids. The importance of the fluid phase for a variety of geological processes is widely accepted (e.g. FYFE et al, 1978; YARDLEY and SHMULOVICH, 1995; TOURET, 2001). An increasing number of contributions presents data on metamorphic fluid inclusions. The majority of fluid inclusion work has been focused on quartz-hosted inclusions for practical reasons such as the frequent occurrence and the low refractive index of quartz. The interpretation of compositional and density data from quartz-hosted fluid inclusions is, however, a matter of debate. Post entrapment modifications such as necking down, changes in volume and leakage of volatile and dissolved species in and out have repeatedly been reported from metamorphic and synthetic fluid inclusions (e.g. ROEDDER, 1984; VITYK and BODNAR, 1995; HOLLISTER, 1990; JOHNSON and HOLLISTER, 1995; BAKKER and DIAMOND, 1998). Comparatively little work has been done on fluid inclusions hosted by metamorphic index minerals such as garnet and kyanite. This is probably due to the fact that fluid inclusions are less frequently observed in these phases and that the inclusions are more difficult to investigate because of the high refractive index of the host minerals. Despite these difficulties, garnet and kyanite have been shown to preserve primary high-grade fluid inclusions without post-entrapment modifications

[1] Institut für Mineralogie und Petrologie, Universität Graz, Universitätsplatz 2, A-8010 Graz, Austria.
<reinhard.kaindl@uni-graz.at>

(TOURET 1981; ELVEVOLD and ANDERSEN, 1993; PHILLIPOT et al., 1995; WHITNEY et al., 1996). Garnet does, however, not always have the desired conservation potential. VRY and BROWN (1991) reported on decrepitation phenomena of garnet-hosted primary fluid inclusions.

We present petrographic, stable isotope and fluid inclusion data from medium grade metapelites from the Radenthein complex of the Austroalpine basement that are indicative of post entrapment modification of garnet- and kyanite-hosted fluid inclusions. In the medium grade metamorphic metapelites of the Radenthein complex several generations of fluid inclusions occur in garnet, kyanite and quartz. Oxygen isotope thermometry and phase petrologic analysis are employed to constrain the conditions of garnet and kyanite growth and associated entrapment of primary fluid inclusions. We then confront these P-T estimates with isochores calculated from microthermometric and Raman spectroscopic measurements on primary fluid inclusions. Systematic discrepancies between thermobarometric estimates and the densities and compositions of primary fluid inclusions point towards post-entrapment modification of garnet- and ky-
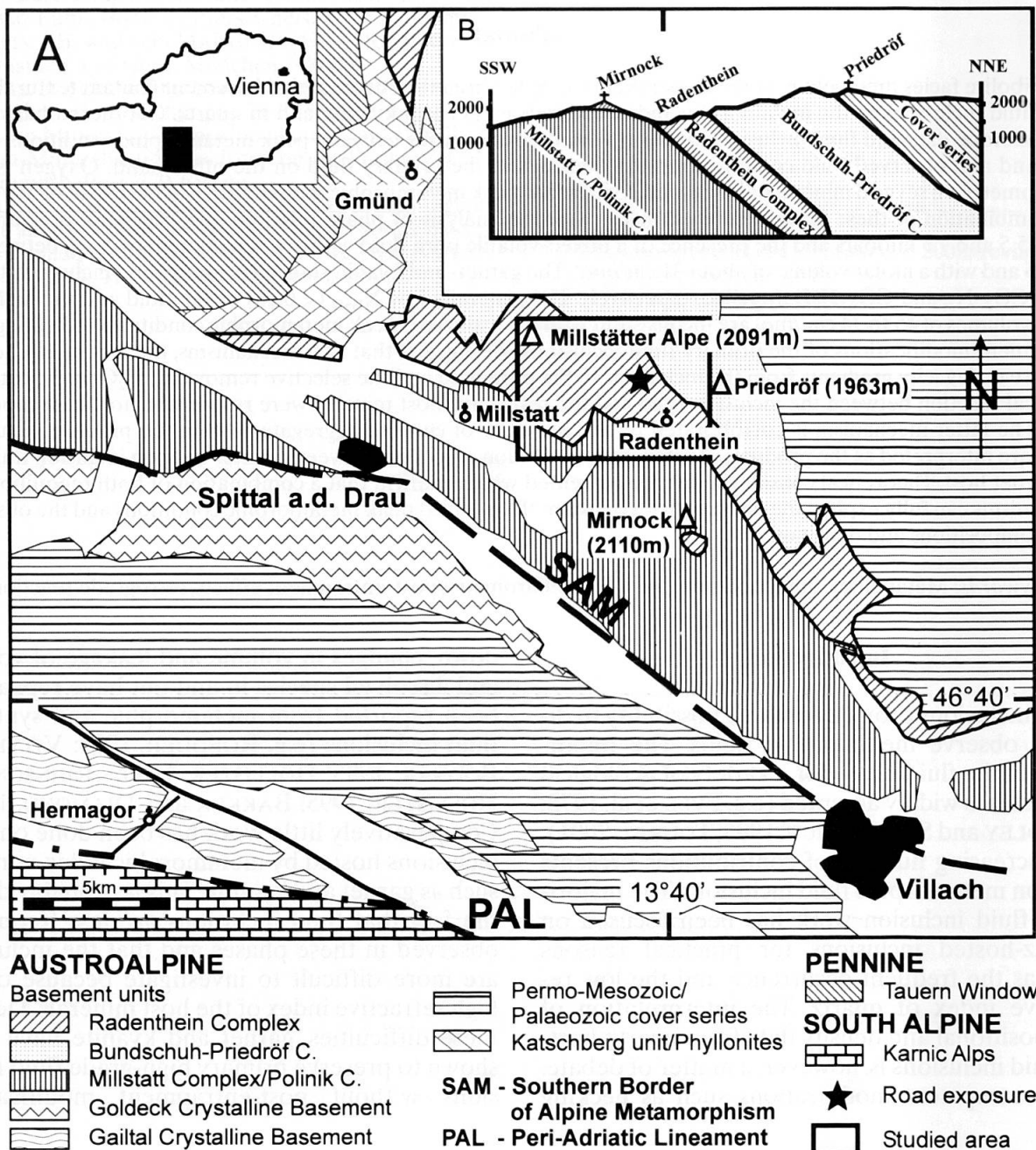

Fig. 1 Simplified geological map and cross section of the Radenthein basement and the regional geology (modified after SCHUSTER and FRANK, 1999).

anite-hosted fluid inclusions. We present petrographic data and theoretical considerations that shed light on the potential mechanisms of such modification.

Geologic setting

The Radenthein complex is located to the southeast of the Tauern Window. A schematic sketch of the regional geology is shown in Fig. 1. The Radenthein complex belongs to the Austroalpine nappe system. It trends approximately east–west and is sandwiched between the Bundschuh-Priedröf complex in the north and the Millstatt complex in the south. As opposed to the adjacent polymetamorphic units, the Radenthein complex only experienced a single medium pressure amphibolite facies overprint during the Cretaceous (SCHIMANA, 1986; HOINKES et al., 1999). The Radenthein unit is primarily comprised of mica schist, garnet-biotite-amphibole schist and amphibolites with subordinate occurrences of metacarbonates such as calcite-dolomite marbles and magnesite. A peculiar coarse grained metapelite variety which locally occurs north of the village of Radenthein is referred to as the "Radentheinit" (AWERZGER and ANGEL, 1948).

Analytical techniques and data reduction

MICROTHERMOMETRY

Microthermometric measurements were done on a LINKAM™ THSMG600 heating and freezing stage equipped with an OLYMPUS™ 80× ULWD objective. Temperatures were calibrated by the melting of CO_2 of synthetic $H_2O–CO_2$ inclusions (–56.6 °C), melting of water ice (0 °C) and critical homogenization (374.1 °C) of synthetic H_2O inclusions in quartz. All measurements were corrected by linear interpolation between temperature deviations at the calibration temperatures (MACDONALD and SPOONER, 1981). The accuracy of measurements was ±0.2 °C at –56.6 °C and 0 °C at a heating rate of 1 °C per minute and ±1 °C at 374 °C and a heating rate of 5 °C per minute. Molar volumes, compositions and isochores were calculated with the computer programs FLINCALC (CAVARRETTA and TECCE, 1995), MacFlinCor (BROWN and HAGEMANN, 1994) and a software package called "FLUIDS" (BAKKER, 2001) and "CLATHRATES" (BAKKER, 1997). The molar volumes for pure N_2 inclusions were taken from the tables of JACOBSEN et al. (1986). The molar volumes of $CO_2–N_2$ inclusions were calculated af-

ter LEE and KESLER (1974) as described in THIERY et al. (1994). The molar volumes and the isochores of $H_2O–CO_2–N_2$ inclusions were calculated using the adaption of BOWERS and HELGESON (1983) for multiple gas mixtures by BAKKER (1999). The molar volumes and isochores of $H_2O–NaCl$ inclusions were calculated after ANDERKO and PITZER (1993).

SCANNING ELECTRON MICROSCOPY (SEM)

Chemical analyses of minerals were done on a JEOL™ 6310 SEM equipped with a LINK ISIS™ energy dispersive system and a MICROSPEC™ wavelength dispersive system. Silicate analyses were done routinely at an acceleration voltage of 15 kV and a beam current of 5 nA. The analyses were corrected for matrix effects (GOLDSTEIN et al., 1992).

MICRO-RAMAN SPECTROSCOPY

Raman spectroscopy was done on an OMARS89 (DILOR™) and on a LabRAM-HR 800 (JOBIN-YVON™) spectrometer. The OMARS89 was used in conjunction with a 5 W argon-laser (excitation lines 514,5 nm and 488 nm), the LabRAM-HR was used with a He-Ne Laser (633 nm) and a He-Cd UV-laser (325 nm). Different excitation wavelengths gave identical results within the analytical error. The system is equipped with an OLYMPUS™ microscope and with 40× UV-, 80× ULWD and 100× objective lenses. The Raman signal is detected with a CCD-camera cooled by liquid-N_2 and the spectra are recorded using the "SCM" technique as described by KNOLL et al. (1990). Beam intensity on the sample surface was about 100 to 200 mW for the OMARS89 and 5 mW for the LabRAM-HR, respectively.

FTIR SPECTROMETRY

Infrared spectra were recorded with a PERKIN-ELMER™ FTIR spectrometer 1760X, equipped with a FTIR microscope having 0.60 numerical aperture mirror lenses (cassegrains) and a liquid-nitrogen-cooled MCT detector in the spectral range between 2500 and 4000 cm⁻¹. Unpolarized background and sample spectra were obtained from 64 scans each in air and in the sample, with 4 cm⁻¹ resolutions. The spot dimension was 100 × 100 μm.

WHOLE ROCK GEOCHEMISTRY

Major element concentrations in whole rock samples were analyzed with ICP-MS by Activation Laboratories Ltd. (Canada).

OXYGEN ISOTOPE ANALYSIS

Mineral separates with a purity of >95% were obtained by magnetic and heavy liquid separation techniques followed by hand picking. Oxygen was extracted from 1 milligram sized samples by means of laser fluorination (SHARP, 1990). The extracted oxygen was cleaned cryogenically and on a KBr absorber at 120 °C. Molecular oxygen was collected on a molecular sieve and finally expanded into a Finnigan-MAT™ Delta^{plus} mass spectrometer for isotope analysis. The external reproducibility of replicate measurements was generally better than 0.15 per mil (1σ).

Petrography of Radentheinite and associated rocks

Most of the samples used in this study were collected from a road cut at Oberfrisnig some 2 kilometers north of the village of Radenthein (Fig.
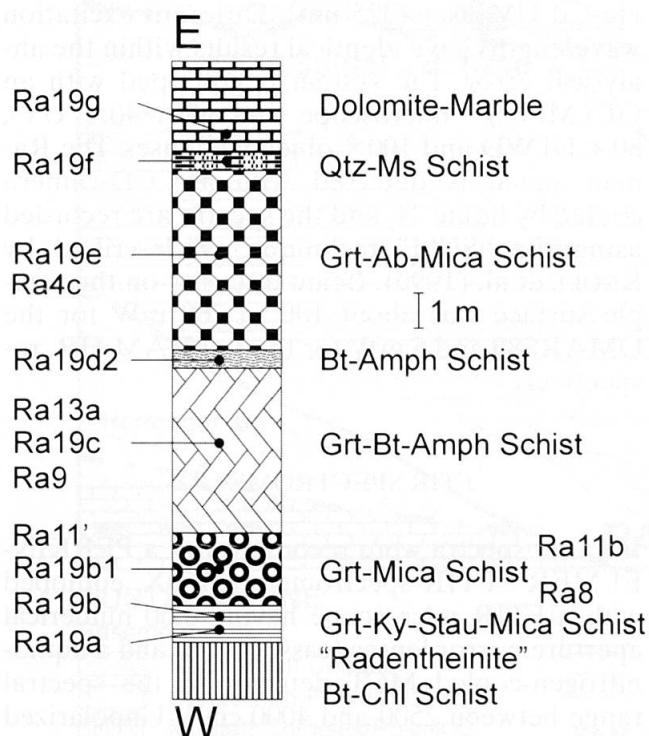

Fig. 2 Schematic litho-stratigraphic sequence of the road cut at Oberfrisnig, 2 km north of the village of Radenthein; from footwall (West) to hanging wall (East). Samples taken from various lithologies are indicated (compare Table 1).

1a). There the Radentheinite forms a layer several meters thick, within a heterogeneous metasediment sequence which is illustrated schematically in Fig. 2. Some samples were taken at the magnesite deposit near Millstätter Alpe. At Oberfrisnig Radentheinite is associated with biotite-chlorite schist, garnet-mica schist, garnet- and biotite-bearing amphibole schist, garnet-albite mica schist, quartz-muscovite schist, and dolomite marble (Fig. 2, Table 1). Except for Radentheinite and the dolomite marble all rocks are strongly foliated, with the foliation subparallel to the compositional layering.

The Radentheinite is a massive, coarse grained rock with a chlorite matrix and up to several centimeter sized porphyroblasts of garnet, kyanite and biotite and occasionally staurolite. The Radentheinite has been mined for its gem quality garnet and as a decorative construction material. The porphyroblasts are idiomorphic and have smooth grain boundaries. They clearly grew over the pre-existing chlorite matrix (Fig. 3). Texturally only one porphyroblast generation is identified and chlorite, garnet, biotite, kyanite and, if present, staurolite belong to the peak metamorphic paragenesis. Garnet is essentially a pure almandine-pyrope solid solution with a subtle Mg/Fe zonation from $X_{Mg} = 0.22$ in the core to $X_{Mg} = 0.28$ in the rims (Table 3). The maximum spessartine content is 5% in the core and decreases outwards. The grossular content is generally below 2%. All other minerals are chemically homogeneous. Representative mineral analyses are given in Table 3.

Bulk rock compositions of the Radentheinite and its country rocks are given in Table 2. As compared to an average pelite composition Radentheinite is particularly rich in aluminum, magnesium, and iron, and it is comparatively poor in silica, calcium and sodium. The garnet-mica schist is enriched in silica, potassium and sodium and depleted in aluminum, iron and magnesium relative to the Radentheinite.

Amphibole, biotite, quartz, ilmenite and garnet are the main constituents of the garnet-biotite-amphibole schist. According to the nomenclature of LEAKE et al. (1997) the amphiboles are mainly tschermakites and subordinately magnesio-hornblendes and alumino-pargasites.

The mineral assemblage garnet-biotite-albite-muscovite-staurolite-kyanite-quartz of the garnet-albite-mica schist is similar to the garnet-mica schist described above. The occurrence of albite and different modal proportions of the phase assemblage distinguish the garnet-albite-mica schist from the garnet-mica schist.

On top of the garnet-albite-mica schist a light fine-grained quartz-muscovite schist of approx. 30 cm thickness, comprised of 50% modal quartz and
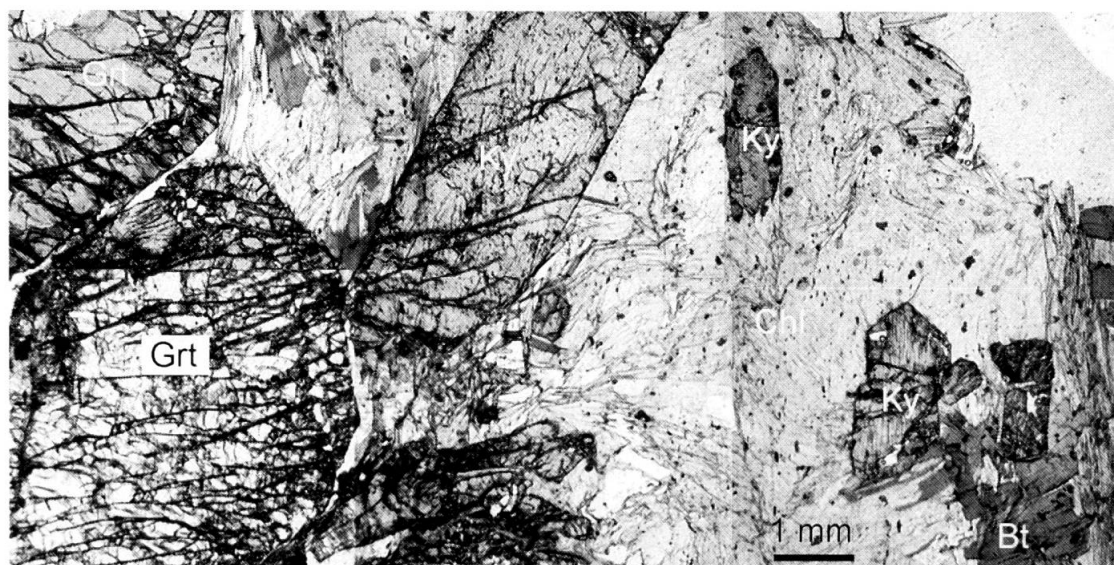
Fig. 3 Compound photomicrograph of the Radentheinite paragenesis; note the euhedral crystal shapes and smooth grain boundaries of garnet (Grt) and kyanite (Ky); biotite (Bt) grows across the chlorite-dominated (Chl) matrix; Grt, Ky and staurolite (not shown) porphyroblasts reach several centimeters in size.

Table 1 Sample number, lithology and paragenesis of the investigated rocks.

Sample Nr.	Lithology	Mineral assemblage
Ra4c	Garnet-albite-mica	grt-ms-bt-ky-qtz-st-pl
Ra8	Garnet-mica	grt-ms-bt-chl-qtz-st
Ra9	Garnet-biotite-amphibole	grt-bt-hbl-chl-pl-czo/ep-qtz
Ra11b	Garnet-mica	grt-ms-bt-ky-qtz
Ra11'	Garnet-mica	grt-ms-bt-chl-ky-qtz
Ra13a	Garnet-biotite-amphibole	grt-bt-hbl-chl-ms-czo/ep-qtz
Ra17a	Garnet-vein	grt-qtz
Ra19a	Radentheinite	grt-bt-chl-ky-qtz
Ra19b	Radentheinite	grt-bt-chl-ky-qtz-st
Ra19b1	Garnet-mica	grt-ms-bt-chl-ky-qtz-st
Ra19c	Garnet-biotite-amphibole	grt-bt-hbl-chl-qtz-pl
Ra19d2	Biotite-amphibole	bt-hbl-qtz-pl-chl
Ra19e	Garnet-albite-mica	grt-ms-bt-chl-pl-ky-qtz-st
Ra19f	Quartz-muscovite	qtz-ms
Ra19g	Dolomite marble	dol-cal

All lithologies schistose except vein and marble.
Mineral abbrevations after KRETZ (1983).

50% modal muscovite, and a granular dolomite marble represent the uppermost section of the road cut at Oberfriesnig.

Thermobarometry

OXYGEN ISOTOPE THERMOMETRY

Three samples, a Radentheinite (Ra19a), a staurolite-kyanite-bearing garnet-mica schist (Ra11') and a quartz-muscovite schist (Ra19f) were chosen for oxygen isotope thermometry. All these samples show equilibrium textures and lack evidence of retrograde mineral reactions. Sample Ra19a and Ra11' contain staurolite. In both cases, however, staurolite hosts abundant quartz-inclusions and clean separates for oxygen isotope analysis could not be obtained. The oxygen isotope data as well as the estimated equilibration temperatures and the calibrations used are given in Table 4. Out of the phases analyzed, garnet, kyanite and quartz have the lowest rates of oxygen volume diffusion (e.g. COLE and OHMOTO, 1986). These phases are expected to yield the most reliable estimates for the peak metamorphic temperatures (e.g. EILER et al., 1993). This is why the thermometric calibrations were chosen such that

Table 2 Bulk rock compositions of the Radentheinite and its associated rocks. For comparison an average shale composition (WEDEPOHL, 1978) is shown.

Rock	Radentheinite	Radentheinite	Grt-Mica	Grt-Bt-Amph	Bt-Amph	Grt-Ab-Mica	Qtz-Ms	Dol-Mar	Average shale
Sample	RA19A	RA19B	RA19B1	RA19C	RA19D2	RA19E	RA19F	RA19G	–
SiO_2	37.95	38.30	59.02	47.26	39.15	53.23	70.39	1.33	58.90
Al_2O_3	26.94	24.37	20.10	14.65	20.23	17.74	16.22	0.67	16.70
Fe_2O_3	13.19	14.20	6.42	14.40	18.84	13.91	0.91	1.22	6.91
MnO	0.07	0.06	0.06	0.13	0.17	0.15	–	0.12	0.09
MgO	12.85	12.76	4.01	6.12	3.34	3.66	1.87	19.80	2.60
CaO	0.22	0.24	0.31	4.96	2.76	2.67	0.13	29.84	2.20
Na_2O	0.25	0.16	0.68	3.98	3.98	2.16	0.15	0.05	1.60
K_2O	1.40	1.46	4.20	1.43	1.47	2.02	5.82	0.23	3.60
TiO_2	1.29	1.00	0.85	4.20	5.79	3.68	0.28	0.02	0.78
P_2O_5	0.14	0.17	0.09	0.56	0.55	0.61	0.09	0.01	0.16
LOI	5.68	5.91	2.95	0.95	2.40	0.92	2.69	45.38	5.00
Total	99.97	98.62	98.69	98.63	98.67	100.74	98.55	98.67	98.54

Lithology and mineral assemblage see Table 1; average shale after WEDEPOHL (1978).

Table 3 Selected mineral compositions of Radentheinite and some associated rocks.

	Radentheinite					Garnet–mica			Grt–Bt–Amph		
	Grt–c.	Grt–r.	Bt	Chl	St	Grt	Bt	St	Grt	Bt	Amph
SiO_2	39.02	38.53	38.64	26.56	27.67	36.53	38.42	27.98	38.16	37.17	42.89
Al_2O_3	20.81	21.01	18.95	23.79	52.57	20.85	19.13	56.00	21.20	18.69	16.06
FeO	32.84	32.72	13.69	18.23	10.92	35.35	13.74	10.68	31.72	17.17	15.12
MnO	2.12	0.67	0.01	–	–	0.90	0.06	–	0.48	–	0.72
MgO	0.64	6.34	15.44	20.44	2.32	3.77	15.25	1.36	3.35	12.91	10.50
CaO	0.43	0.52	0.14	–	0.02	0.81	0.01	–	5.26	0.01	10.35
Na_2O	–	–	0.33	0.01	0.12	–	0.41	–	–	0.23	1.98
K_2O	–	–	8.20	–	–	–	7.43	–	–	9.26	0.26
TiO_2	–	–	1.44	0.23	0.45	0.02	1.34	0.37	0.12	1.18	0.47
ZnO	–	–	–	–	2.31	–	–	2.60	–	–	0.01
Total	100.72	99.79	96.98	89.34	96.38	98.23	95.79	98.99	100.30	96.62	98.35
Ox.nr.	12	12	22	12	46	12	22	46	12	22	23
Si	3.07	3.04	5.54	2.63	7.79	2.98	5.55	7.64	3.02	2.74	6.21
Al	1.93	1.95	3.20	2.78	17.44	2.01	3.26	18.02	1.98	1.63	2.74
Fe^{2+}	2.16	2.16	1.64	1.51	2.57	2.38	1.66	2.44	2.10	1.06	1.24
Fe^{3+}	–	–	–	–	–	0.03	–	–	–	–	0.59
Mn	0.14	0.05	–	–	–	0.06	0.01	–	0.03	–	0.09
Mg	0.64	0.75	3.30	3.02	0.97	0.46	3.28	0.55	0.40	1.42	2.27
Ca	0.04	0.04	0.02	–	0.01	0.07	–	–	0.45	0.00	1.60
Na	–	–	0.09	0.00	0.07	–	0.12	–	–	0.03	0.56
K	–	–	0.75	–	–	–	1.37	–	–	0.87	0.05
Ti	–	–	0.16	0.02	0.10	0.00	0.15	0.08	0.01	0.07	0.05
Zn	–	–	–	–	0.48	–	–	–	–	–	–
Sum	7.97	7.98	14.70	9.96	29.43	7.99	15.38	28.73	7.98	7.82	15.38

Grt-c.: garnet-core; Grt-r.: garnet-rim; Ox.nr.: number of oxygens used for calculations.

internal consistency among these phases is guaranteed. For quartz-kyanite fractionations the empirical calibration of SHARP (1995) and for quartz-garnet, the calibration of RICHTER and HOERNES (1988) were used, accordingly. For quartz-biotite and quartz-muscovite the calibrations of ZHENG (1993) were used.

All oxygen isotope thermometers yield temperatures in the range of 560° to 590 °C, which are concordant within the uncertainty of the method. This suggests that oxygen isotope equilibrium was attained at peak metamorphic temperatures in the range of 560° to 590 °C and that the peak metamorphic fractionations are preserved. The temperature estimates from oxygen isotope ther-

Table 4 Oxygen isotope compositions of quartz, muscovite, biotite, kyanite and garnet within Radentheinite, garnet-mica schist and quartz-muscovite schist. The uncertainty of the inferred equilibrium temperatures is based on the analytical uncertainty of the oxygen isotope compositions of the individual minerals.

Sample	Mineral	$\delta^{18}O$ (‰)	mean	σ_1	$\delta_{qtz-min}$ (‰)	σ_2	T–1σ	T	T+1σ	Reference
	Qtz	14.64	14.59	0.07	–	–	–	–	–	
	Qtz	14.54								
	Gt	10.37								
Ra19b	Gt	10.21	10.19	0.18	4.40	0.26	542	566	592	RICHTER and HOERNESS
	Gt	10.00								(1988)
	Bt	10.95	10.93	0.04	3.67	0.11	574	589	605	ZHENG (1993)
	Bt	10.90								
	Ky	11.73	11.60	0.18	2.99	0.25	545	579	617	SHARP (1995)
	Ky	11.47								
	Qtz	14.15	14.23	0.11	–	–	–	–	–	
	Qtz	14.30								
	Gt	9.80	9.75	0.07	4.48	0.18	542	559	576	RICHTER and HOERNESS
Ra11'	Gt	9.70								(1988)
	Bt	10.36	10.43	0.10	3.80	0.21	544	570	595	ZHENG - Annite (1993)
	Bt	10.50								
	Ky	11.42	11.34	0.12	2.89	0.23	561	593	613	SHARP (1995)
	Ky	11.25								
	Qtz	17.63	17.74	0.15	–	–	–	–	–	
Ra19f	Qtz	17.84								
	Ms	14.94	14.95	0.01	2.79	0.16	529	557	588	ZHENG (1993)
	Ms	14.95								

σ_1: standard deviation $\delta^{18}O$; $\delta_{qtz-min}$: isotope fractionation between quartz and mineral.
σ_2: standard deviation of isotope fractionation.
T–1σ: equilibrium temperature in °C minus standard deviation.
T: equilibrium temperature in °C.
T+1σ: equilibrium temperature in °C plus standard deviation.

mometry are largely independent of pressure and fluid composition.

PHASE DIAGRAM CALCULATIONS

The chemical composition of the Radentheinite is constant over the sampled area (see Table 2). Together with the fact that only one generation of metamorphic minerals is present and that – with the exception of slightly zoned garnet – the minerals are chemically homogeneous, this facilitates analysis of phase relations in a pseudosection rather than in a petrogenetic grid. In the Radentheinite, the components CaO, MnO, and Na$_2$O only occur at <0.25 wt% levels, and these components are disregarded in our analysis. A pseudosection for the Radentheinite composition in the simplified model system SiO_2–Al_2O_3–MgO–FeO–K_2O–H_2O–CO_2 is illustrated in Fig. 4. The diagrams were constructed using the program package PeRpLeX (CONNOLLY, 1990) and the thermodynamic data of HOLLAND and POWELL (1990). Calculations were done for a quartz, aluminosilicate and H_2O–CO_2 fluid saturated system. Trivariant fields are shaded in grey, areas without

shading represent divariant fields. The typical Radentheinite paragenesis is represented by the chlorite + garnet + biotite divariant field in Fig. 6a. Within this field, the compositions of the chlorite, biotite and garnet solid solutions vary as a function of pressure and temperature. For chlorite the compositional variation is very subtle, but for garnet and biotite significant compositional variations are predicted over their stability fields. The portions of the chlorite + garnet + biotite (+ quartz + kyanite) divariant field with garnet and biotite compositions that match the observed compositions are shaded in dark grey in Fig. 4a. Towards low temperatures this field is bounded by the chlorite + biotite + staurolite (+ kyanite + quartz) divariant field, which has a comparatively limited extension in the P-T diagram. The fact that staurolite is observed in some of the Radentheinite samples, suggests that the prograde P-T path passed through this divariant field. A high-pressure limit for the peak metamorphic conditions is given by the alumina content of biotite (Al/(Al+Fe+Mg)) = 0.23). A low-pressure limit is given by the lower stability limit of kyanite. A high temperature limit is given by the X_{Mg} in garnet and biotite ($X_{Mg}^{Gt} = 0.3$, $X_{Mg}^{Bt} = 0.7$).

Table 5 Petrographic and microthermometric properties of fluid inclusions in the Radenthein complex.

Type	Host	System	Phases	Class	T_i	Tm_{ice}	Tm_{CO_2}	Th_{CO_2}	Tm_{clath}	Th_{tot}	Ts_{hal}	MV	Sample
1a	Grt	N_2	L	single						−160		47	Ra4c
1b	Qtz	N_2	L	cluster, trails						−164/−153		44/54	Ra4c
2a	Grt	CO_2-N_2±CH_4+H_2O	L+V	cluster, trails			−60.6/−59.8	+7/+13				ca. 70	Ra4c
2a	Grt	CO_2-N_2-H_2O	L+V	single, cluster			−57.6	23.8				49	Ra9
2a	Grt	CO_2-N_2±H_2O	L,L+V	single, cluster			−58.5/−56.9	0.9/30.2				41/57	Ra11'
2a	Grt	CO_2-N_2±H_2O	L+V	single, cluster			−58.9/−56.6	23.8/29.4				50/55	Ra13a
2a	Grt	CO_2-H_2O±N_2	L,L+V	single, trails			−58.8/−57	−10.7/30				47/62	Ra19a
2a	Grt	CO_2-N_2±H_2O	L,L+V	single, trails			−58.8/−57.7	27.5/29.3				52/55	Ra19e
2a	Grt	CO_2-N_2±H_2O	L+V	trails			−60/−57.7	10/29.6				47/55	Ra17a
2a	Grt	CO_2-N_2±CH_4+H_2O	L,L+V	cluster, trails			−57.8/−56.6	13.9/25.2				46	Ra4c
2b	Ky	CO_2-N_2-H_2O	L1+L2	z–parallel, cluster, trails			−61.3/−56.9	−0.3/27.1	10/15	186/235		41/42	Ra11b
2b	Ky	CO_2-N_2-H_2O	L1+L2	z–parallel, trails			−58.8	2.2				22	Ra11'
2b	Ky	CO_2-N_2-H_2O	L1+L2	z–parallel, trails			−59.1/−56.9	2.1/17.7				41/59	Ra19a
2b	Ky	CO_2-N_2±H_2O	L+V	z–parallel, cluster, trails			−57.5/−57.1	22.5/25.1	10.3			48/49	Ra19e
2c	Qtz	CO_2-N_2-H_2O	L1+L2	cluster, trails			−62.6/−56.6	−31/+25				49/74	Ra4c
2c	Qtz	CO_2-N_2	L,L+V	trails			−58.1/−57.6	−19/−3				46/51	Ra8
2c	Qtz	CO_2-N_2	L	cluster, trails			−59/−57.2	−27.9/10.8				42/53	Ra13a
2c	Qtz	CO_2-N_2	L,L+V	cluster, trails			−58.7/−58	−0.5/22.9				22/31	Ra11b
2c	Qtz	CO_2-N_2	L	cluster, trails			−56.8	29.1				70	Ra19e
2c	Qtz	CO_2	L	single			−59.4	6				26	Ra8
2d	Qtz	CO_2-H_2O-N_2	L1+L2	single		−10.4	−58.8/−58	−59.5/10.6	9			55/62	Ra11b
2d	Qtz	CO_2-N_2-H_2O	L1+L2	cluster, trails			−59.2/−58.7	7.1/13.2	5.6/9.4			22/24	Ra11'
2d	Qtz	CO_2-H_2O	L1+L2	trails		−0.7	−56.8	−5.8/1.8	6.4/8.5			19/40	Ra19e
3a	Grt	H_2O	L+V	single		−0.8				340		30	Ra17a
3b	Qtz	H_2O-NaCl-$FeCl_2$	L+V	trails	−35/−33	−13/−11							Ra4c
3b	Qtz	H_2O-NaCl-$FeCl_2$	S+L+V	single						201	215	21	Ra4c
3b	Qtz	H_2O-NaCl-$FeCl_2$	L+V	trails	−37/−38	−10				230/261		21/22	Ra8
3b	Qtz	H_2O-NaCl	L+V	trails		−18/−9							Ra9
3b	Qtz	H_2O-NaCl	L+V	cluster, trails	−20	−3/−4				250/299		22/24	Ra11b
3b	Qtz	H_2O-NaCl-$CaCl_2$	L+V	cluster, trails	−56	−24/−23				238/314		21/23	Ra13a

L: liquid; V: vapor; L1, L2: immiscible liquids; S: solid; Grt: garnet; Ky: kyanite; Qtz: quartz; Ti: initial melting; Tm_{ice}: ice melting; Tm_{CO_2}: CO_2 melting; Th_{CO_2}: CO_2 homogenization; Tm_{clath}: clathrate melting; Th_{tot}: total homogenization; Ts_{hal}: halite melting; MV: molar volume min/max (cm^3/mol).
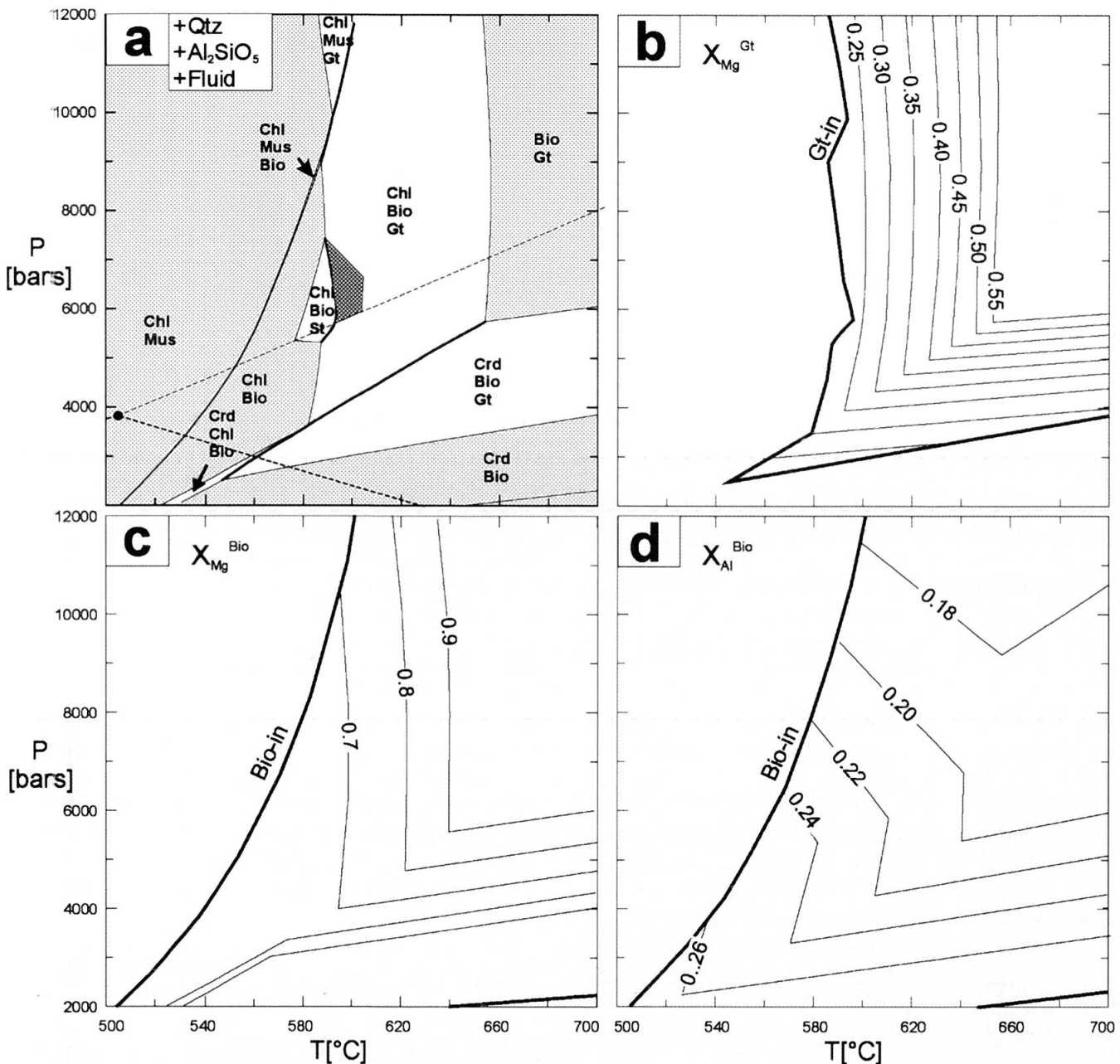
Fig. 4 (a) Phase diagram section for the simplified SiO_2–Al_2O_3–MgO–FeO–K_2O–H_2O–CO_2 model system for the Radentheinite composition as given in Table 3 and for $X_{H2O} = 0.46$. Trivariant fields shaded in gray, divariant fields without shading; stability fields are labeled with the respective paragenesis, aluminous silicate stability is indicated by dashed lines. The dark gray shaded field indicates the chlorite + garnet + biotite divariant field combined with garnet and biotite compositions that match the observed compositions. (b) X_{Mg} isopleths for the garnet solid solution; (c) X_{Mg}, and (d) $X_{Al/(Al+Fe+Mg)}$ isopleths for the biotite solid solution. See text for more details about diagram construction and discussion.

The positions of the individual di- and trivariant fields with respect to the temperature axis are sensitive to the partial pressure of water in the fluid phase. Depending on the paragenesis under consideration, the limits of the individual stability fields may be shifted over 10° to 30 °C by a change of 0.1 units in X_{H2O}. The temperature estimate in Fig. 6a agrees best with the temperatures derived from oxygen isotope thermometry for an X_{H2O} of 0.46. We regard this composition being the best representative of the peak metamorphic pore fluid. This is why we conclude from oxygen isotope thermometry combined with phase diagram calculations that peak metamorphic conditions were about 560° to 590 °C and 5.5 to 7.5 kbars. The water fugacity appears to have been significantly reduced with respect to pure water so that X_{H2O} is estimated to have been in the range of 0.4 to 0.5.

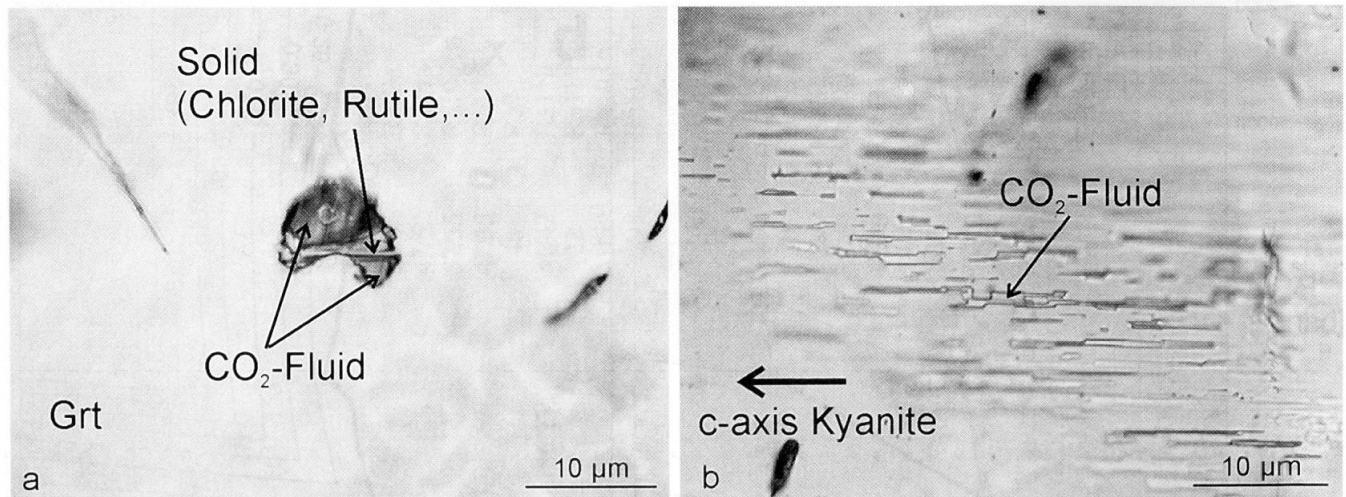*Fig. 5* Photomicrograph of (a) CO_2–N_2 (Type 2a) inclusion in garnet in Radentheinite. The right hand side of the inclusion contains the fluid phase; bright areas are solid phases and thin walls within the inclusion, respectively. (b) Primary CO_2–$N_2\pm H_2O$ (Type 2b) inclusions in kyanite from Radentheinite. The inclusions are roughly negative-crystal shaped and elongated parallel to the c-axis of the host crystal. Two larger inclusions, marked by arrows, contain a CO_2–N_2 supercritical fluid and are essentially water free. The major part of the marked inclusions is filled by a solid phase aggregate.

Fluid inclusions

Based on the fluid composition and host mineral we distinguish three types of fluid inclusions (Table 5): (1) Pure N_2 inclusions in garnet (Type 1a) and in quartz (Type 1b); (2) CO_2–$N_2\pm CH_4$ inclusions in garnet (Type 2a) and CO_2–$N_2\pm CH_4\pm H_2O$ in kyanite (Type 2b) and in quartz (Type 2c); (3) H_2O inclusions in garnet (Type 3a) and H_2O-$NaCl\pm CaCl_2\pm FeCl_2$ inclusions in quartz (Type 3b). According to KERKHOF and HEIN (2001) the terminology proposed by SIMMONS and RICHTER (1976) and KRANZ (1983) for the classification of fluid trails was used.

TYPE 1: N_2 INCLUSIONS IN GARNET AND QUARTZ

The least frequent fluid inclusions are pure, isolated N_2 inclusions in the cores of garnet porphyroblasts within Radentheinite (Type 1a). They are dark and irregularly shaped and have a diameter of about 5 μm. During heating after cooling to –190 °C the only phase transition observed is homogenization to the liquid (L + V → L). These inclusions are classified as Type H1 after KERKHOF (1988), accordingly. On cooling, a vapor bubble appears at around –160 °C, which homogenizes after a few degree of heating. Intragranular N_2 inclusions in the cores of quartz grains in Radentheinite and garnet-biotite-amphibole schist (Type 1b) are more frequent. They are arranged in clusters and irregularly shaped ranging from 4 to 9 μm in diameter. They homogenize to the liquid at temperatures between –162° and –153 °C. N_2 is the only volatile species, which is detected by Raman spectroscopy. Their molar volume $\bar{V}$ ranges between 45 and 53 cm^3/mol. The N_2 in these inclusions was probably derived from NH_4^+, which may be incorporated in mica and feldspar at low temperature and disintegrates to N_2 and H_2 at higher temperature (BEBOUT and FOGEL, 1992).

TYPE 2: CO_2–$N_2\pm CH_4$ INCLUSIONS IN GARNET, KYANITE AND QUARTZ

Type 2a CO_2–$N_2\pm CH_4$ inclusions occur isolated, as small clusters or along intragranular trails in garnet porphyroblasts of Radentheinite, garnet-mica schist, garnet-biotite-amphibole schist and garnet-albite-mica schist. The size of the vermicular, flat and irregular or rod-shaped intragranular inclusions trails varies from 4 to 20 μm. (Fig. 5a). The vermicular varieties resemble primary CO_2–N_2 fluid inclusions in garnet observed by ELVEVOLD and ANDERSEN (1993).

Three phase transitions can be observed during heating runs (H3 inclusions; KERKHOF, 1988): melting of CO_2 and formation of liquid (Tm_{CO_2}; S + V → S + L + V → L + V) and homogenization into the liquid and sometimes into the vapor phase (Th_{CO_2}; L + V → L or V). Tm_{CO_2} ranges from –60.6 °C to –56.6 °C (Fig. 6a) indicating variable fluid compositions. Raman spectroscopy yielded variable N_2 contents of up to 10% in the homogeneous fluid phase. Few inclusions contain ternary
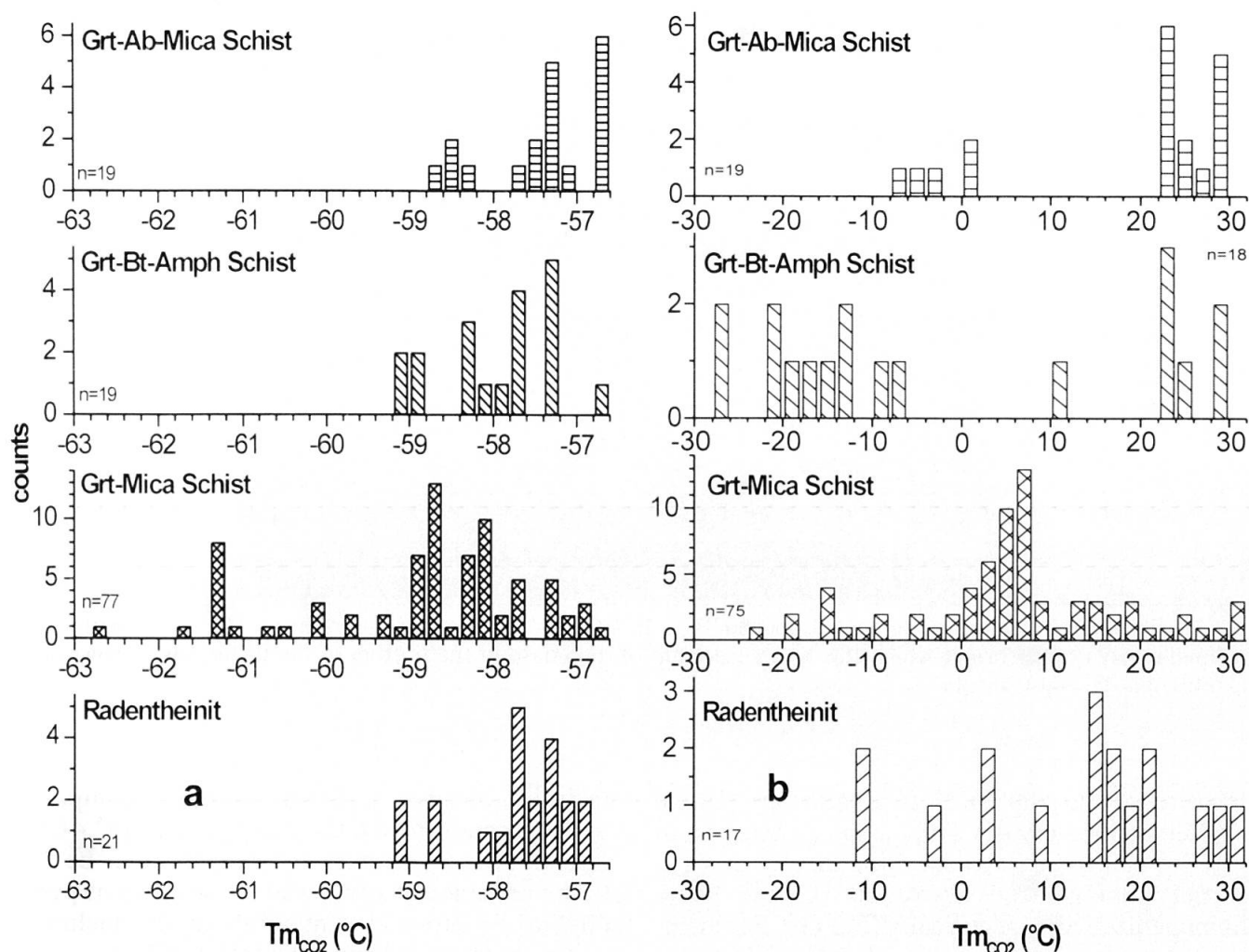
Fig. 6 (a) Initial melting temperature (Tm_{CO_2}) histograms for carbonic inclusions ($\pm H_2O$) occurring in the Radentheinite and its country rocks. The low melting temperatures in the garnet-mica schist below –61 °C are the result of ternary CO_2–N_2–CH_4 fluid compositions (see text). The carbonic phase of inclusions in the other lithologies melts at higher temperatures and contains N_2 but no detectable CH_4. (b) Homogenization temperature (Th_{CO_2}) histograms for carbonic inclusions ($\pm H_2O$). The Th_{CO_2} differences between the lithologies are related to the occurrence of the inclusions in different host minerals: most of the Th_{CO_2} above 15 °C in the garnet-albite-mica schist, the garnet-biotite-amphibole schist and the Radentheinite were measured on inclusions in garnet and kyanite; most inclusions in the garnet-mica schist occur in quartz and homogenize between 0 and 8 °C.

Table 6 Molar proportions, volumes and activities of the phases involved in reaction (1).

Phase	X_{Mg}	a_{Solid}	X_{H2O}	a_{H2O}	$\overline{V}$(cm³/mol)	V (cm³)
Pyrope	0.3	0.027	1	1	113.15	62.16
Clinochlore	0.72	0.149	0.8	0.86474	210.9	38.62
Amesite	0.72	0.043	0.6	0.74768	209.8	38.42
Quartz	1	1	0.46	0.63791	22.69	16.62
–	–	–	0.4	0.58063		
–	–	–	0.2	0.33680		
–	–	–	0.1	0.18087		
–	–	–	0.01	0.01925		

X_{Mg}: Molar proportions for the component in solid solution. a_{Solid}: Activity of component in solid solution. X_{H2O}: Molar proportion of water in a mixed CO_2–H_2O fluid. a_{H2O}: Water activity in a mixed CO_2–H_2O fluid at 570 °C and 6.5 kbar (KERRICK and JACOBS, 1981). $\overline{V}$: molar volumes of solids (HOLLAND and POWELL, 1990). V: Volume of solids inside a hypothetical 100 cm³ inclusion after completion of reaction (1).

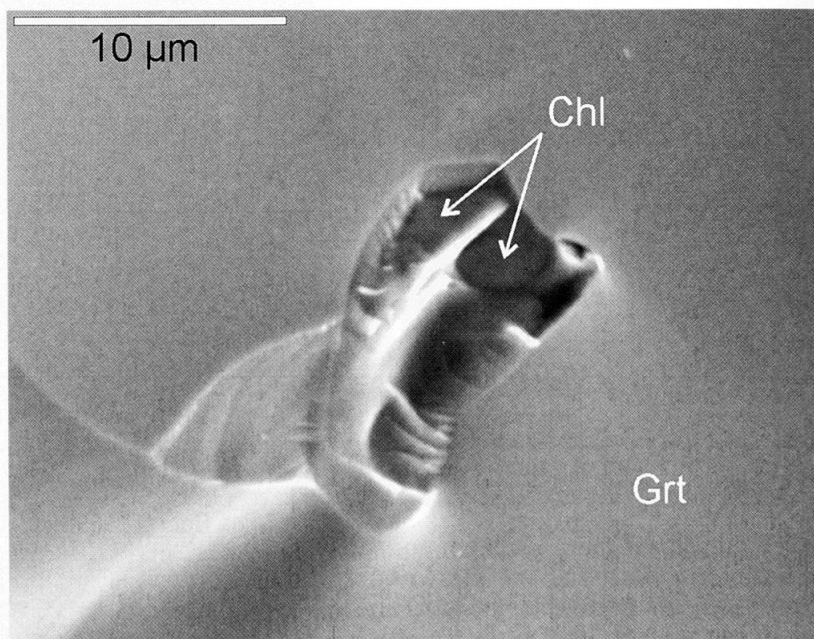*Fig. 7* Secondary electron image of an opened Type 2a CO_2–N_2 fluid inclusion in garnet. Thin walls within the opened cavity appear bright white; the X-ray spectrum of the phase in the bottom of the inclusions (arrows) was identified as Fe-Mg-Chlorite.

mixtures of CO_2 (80%), N_2 (6%) and CH_4 (14%), explaining the very low Tm_{CO_2}. Th_{CO_2} ranges from –10.7 to +30.2 °C, the majority of the inclusions in garnet homogenized above 20 °C and some homogenized almost critically (Fig. 6b). For inclusions homogenizing into the liquid high molar volumes in the range of 45 to 74 cm^3/mol were calculated from homogenization temperatures and Raman analyses of the gas composition. Calculations were done with the software of BAKKER (2001), which combines the findings of THIERY et al. (1994) and the equations of LEE and KESLER (1974).

In many cases fluid occupies only part of the inclusion volume. Large fractions of the inclusions may be filled with birefringent solid phases. In order to identify these phases, garnet and kyanite host crystals were chipped and coated with graphite and then analysed on the secondary electron microscope (SEM; METZGER et al., 1977). Crater-like, uneven structures on SEM-images of chipped garnets are interpreted as opened fluid inclusions, from which all vapor and liquid phases have evaporated, whereas the solid phases have remained (Fig. 7). In several instances Fe-Mg-sheet silicates and a TiO_2 polymorph could be qualitatively identified on the SEM. Salt daughter crystals were not observed. We assume that the observed structures represent opened Type 2b carbonic inclusions. Raman spectroscopy of the solid inclusion phases point towards the presence of chlorite (Fig. 8). The Raman peaks of the solid

inclusion phases are slightly shifted as compared to matrix chlorite and the sharp peak at 192.4 cm^{-1} does not occur in matrix chlorite. This may be due to the presence of additional phases such as pyrophyllite or other clay minerals in the inclusion and/or to chemical and orientation effects.

Kyanite contains primary and pseudosecondary CO_2–N_2±CH_4±H_2O inclusions (Type 2b; Table 5). Primary inclusions within idiomorphic kyanite are elongated with an average length of 5 µm and arranged parallel to the c-axis of the host (Fig. 5b). Pseudosecondary inclusions trails in kyanite are rounded without preferred orientation and occur in planes more or less perpendicular to the c-axis. At room temperature the majority of the inclusions contain one or two liquids and an optically unidentifiable solid phase. The two liquids turned out to be CO_2 and H_2O. The degree of fill of the aqueous phase (DF_{H_2O}) varies from 0 (pure CO_2) to 0.26 at the homogenization temperature of CO_2. Several phase transitions after cooling below 95 °C and reheating can be observed in three-phase CO_2–H_2O inclusions starting with the triple point melting of solid CO_2 (Tm_{CO_2}) in the carbonic subsystem (S_{CO_2} + ICE + V → S_{CO_2} + L_{CO_2} + ICE + V → L_{CO_2} + ICE + V) between –61.3 and –56.6 °C (Fig. 6a). The lowest Tm_{CO_2} were measured for inclusions in samples from the garnet-mica-schist. Raman analysis of the homogenous gas phase yielded N_2 contents of up to 11 mol%. Clathrate, which usually grows during reheating of rapidly cooled CO_2–H_2O inclusions out of ice and gas,
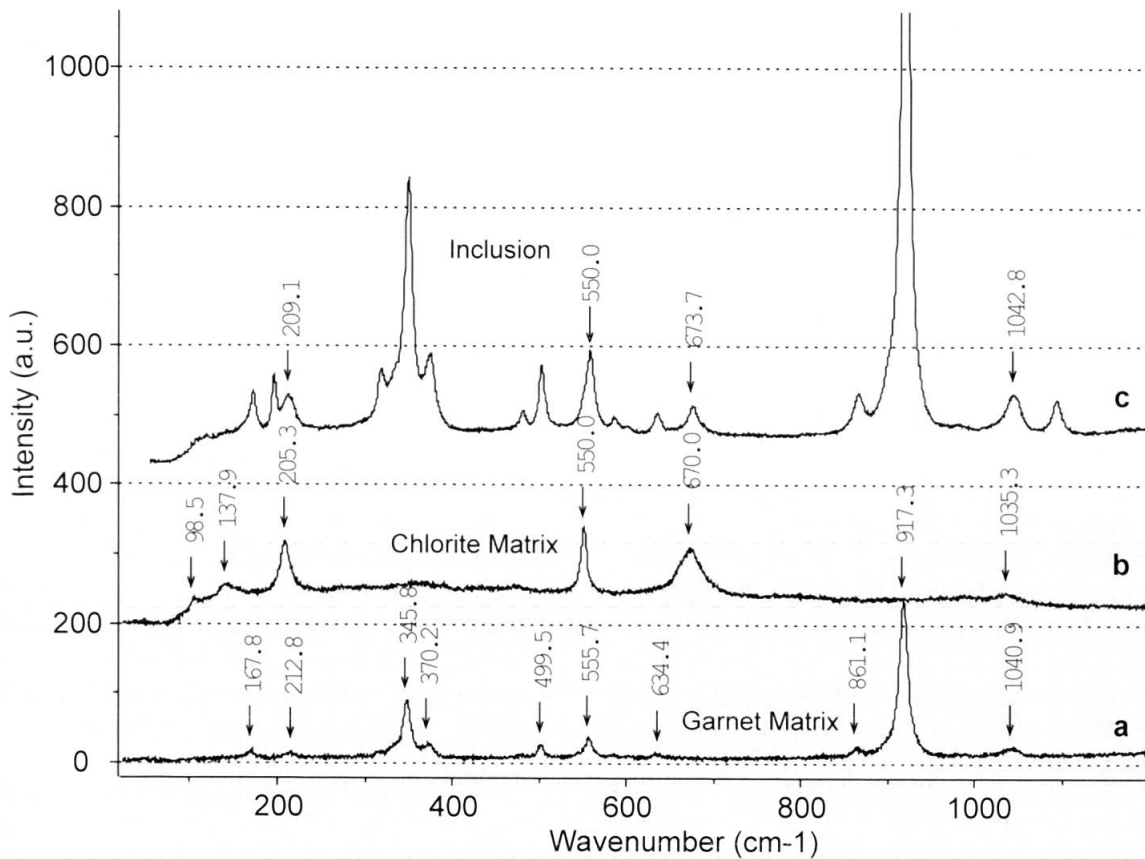
Fig. 8 Raman spectrum of (a) garnet hosting Type 2a CO_2–N_2 inclusions, (b) large chlorite crystal in the matrix and (c) a solid phase within a Type 2a CO_2–N_2 inclusion in garnet. See text fur further explanations.
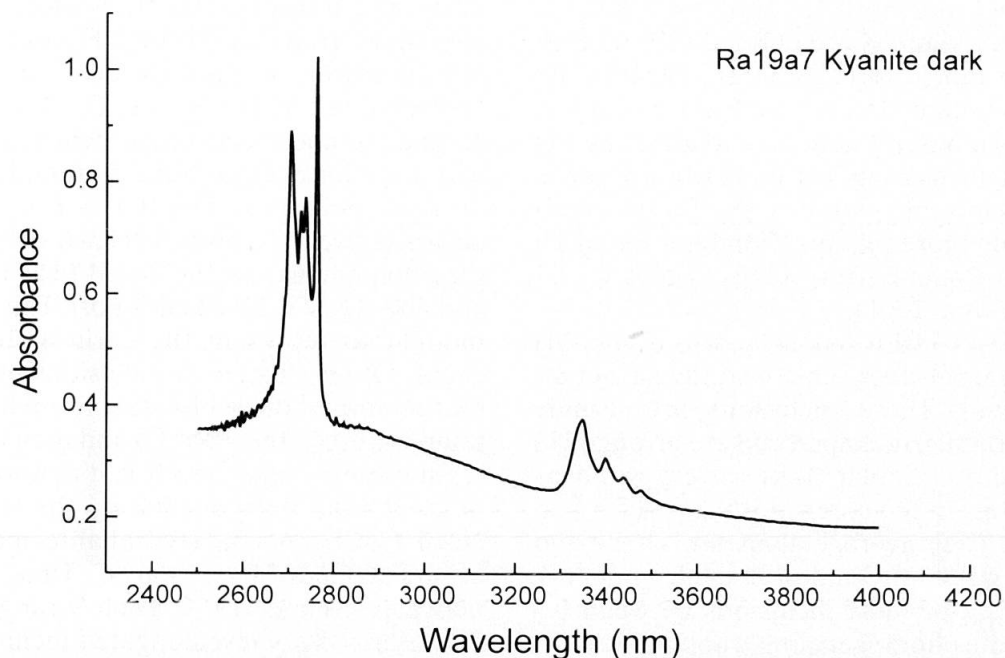

Fig. 9 FTIR spectrum of dark clouded areas within kyanite in Radentheinite. Peaks between 2600 and 2800 cm^{-1} are typical for vibrational modes of OH molecules in sheet-silicates.

melts between +9° to +10 °C (Tm_{CLATH}; CLATH + L_{CO_2} + L_{H_2O} + V → L_{CO_2} + L_{H_2O} + V). Homogenization of the carbonic phase Th_{CO_2} occurs over a large temperature range between –0.3 and + 27.1 °C (Fig. 6b). In some cases total homogenization

Th_{TOT} (L_1 + L_2 → L) of CO_2–N_2–H_2O inclusions could be observed between 186° and 235 °C. Molar volumes between $\bar{V}$ = 31 to 36 cm³/mol were calculated with the software package CLATHRATES (BAKKER, 1997). Accuracy of $\bar{V}$ is limited

by the uncertainties in estimation of the volume percent of the aqueous phase which wets the inclusion walls.

Fracture fillings and dark clouded domains in kyanite were identified as sheet silicates by SEM investigations and by FTIR-spectroscopy, which yielded peaks between 2600 and 2800 cm^{-1} typical for OH molecules in sheet silicates (Fig. 9). However, structures comparable to the crater-like opened inclusions in garnet, could not be observed. Identification of the solids inside Type 2b inclusions in kyanite by Raman spectroscopy failed due to fluorescence of the kyanite host and small inclusion size.

Rounded to idiomorphic CO_2–N_2±CH_4 inclusions in quartz (Type 2c) from the garnet-biotite-amphibole schist, garnet-mica schist and garnet-albite-mica schist (diameter 3 to 15 μm) are arranged in clusters, intra- and transgranular trails. During heating/freezing runs, three phase-transitions can be observed (H3 inclusions). Very low Tm_{CO_2} down to –62.6° (Fig. 6a) are in accordance with Raman spectroscopy which yielded variable proportions of CO_2 (80-100 mol%), N_2 (0–8 mol%) and CH_4 (0–16 mol%). Th_{CO_2} is highly variable from –31 to +29 °C (Fig. 6b). One inclusion with 4% N_2 in the garnet-mica schist homogenizes to the liquid immediately above Tm_{CO_2} at –59.7 °C. For this inclusion both Tm and Th are known, that means that $\bar{V}$ and X are defined ($\bar{V} \sim$ 40 cm^3/mol; $X_{N_2} \sim$ 15 mol%; THIERY et al., 1994b). The different N_2-content derived by Raman analysis and microthermometry may be explained by (1) inaccuracy of measuring Tm or (2) the possible formation of clathrate hydrates. The Raman analysis is probably more reliable. Combination of Th and X_{N_2} (from Raman spectroscopy) yields $\bar{V}$ = 37 cm^3/mol (BAKKER, 2001).

CO_2–N_2–H_2O inclusions in quartz (Type 2d) occur in the garnet-mica schist and the garnet-albite-mica schist. These inclusions are usually rounded to irregularly shaped and are arranged in clusters and intragranular trails or very rarely as single inclusions in the cores of weakly deformed quartz grains. Their average diameter is 8 μm and they are devoid of any kind of daughter mineral. Uniform DF_{H_2O} of most inclusions between 0.6 and 0.5 indicates homogeneous trapping; few inclusions of variable DF_{H_2O} within one cluster or intragranular trail (DF_{H_2O} = 0.2-0.9) may reflect local fluid heterogeneity or inclusion changes after trapping. The N_2 content of the carbonic phase varies between 3 and 5 mol% N_2 (Tm_{CO_2} –59.4° to –58.7 °C) in inclusions in garnet-mica schist, and the fluid is pure CO_2 in inclusions in garnet-albite-mica schist (Fig. 6a). Tm_{CLATH} ranges from +5.6° to +10.3 °C, Th_{CO_2} was observed between +5.8° to +13.2 °C (Fig. 6b). The salt content of the aqueous phase, calculated with the CLATHRATES package (BAKKER, 1997) varies from 0 to ~12 wt% NaCl. The bulk molar volume was in the range of 22 to 40 cm^3/mol.

TYPE 3: AQUEOUS INCLUSIONS IN GARNET AND QUARTZ

A generation of garnet-hosted aqueous inclusions occurs in almost monomineralic garnet domains of garnet-biotite-amphibole schist (Type 3a). These inclusions are irregularly shaped, flat and have an average size of 10 μm. At room temperatures, they contain a liquid and a vapor phase. During reheating of the frozen inclusion from –60 °C, ice melts at –0.8 °C (ICE + L + V → L + V), indicating a virtually pure H_2O fluid and homogenization to the liquid phase occurrs at 340 °C (L + V → L). $\bar{V}$ is 30 cm^3/mol. Age, origin and relation of these inclusions to the other garnet-hosted carbonic inclusions is unclear.

Aqueous inclusions in quartz occur in the garnet-mica schist and the garnet-biotite-amphibole schist (Type 3b). The inclusion morphology, size and texture are diverse, varying from idiomorphic to irregular, from 4 to 11 μm and from clusters to intra- and transgranular trails indicating a complex fluid trapping history. Hydrohalite within low salinity inclusions melts at around –20 °C (Te; Hydrohalite + ICE + V → ICE + L + V) and over a small temperature range, which is consistent with the binary H_2O–NaCl system. Final melting of these inclusions (Tm; ICE + L + V → L + V) occurs between –3 and –4 °C (~6 wt% NaCl) and they homogenize to the liquid (Th) between 250 and 300 °C ($\bar{V}$ = 22–24 cm^3/mol). This subgroup is thought to represent the earliest fluid-trapping event. Other clusters of inclusions in the garnet-biotite-amphibole schist start to melt at very low temperatures (Te ~ –55 °C) and melt over a larger temperature range, which is diagnostic for three or more fluid components, e.g. the ternary H_2O–NaCl–$CaCl_2$ system. Hydrohalite melting Tm_{HH} occurs around -31 and -36 °C, Tm_{ICE} is very low between –24 and –19 °C. Their $\bar{V}$ range from 22 to 24 cm^3/mol. Very few elongated inclusions, probably the result of necking down, contain a halite daughter crystal, which dissolved in one case at 215 °C. The vapor bubble disappeared at around 200 °C. Transgranular inclusion trails in the garnet-mica schist represent presumably the latest inclusion generation. The first phase transition was measured around –35 °C which corresponds with the eutectic temperature of the ternary H_2O–NaCl–$FeCl_2$ or $MgCl_2$ system. Tm_{ICE} around

–12 °C and Th between 195 and 200 °C results in $\overline{V}$ around 21 cm³/mol.

Discussion

Based on petrographic evidence, we suggest that Type 2 fluid inclusions in garnet and kyanite of the Radenthein complex are primary in origin. Garnet and kyanite belong to the peak metamorphic paragenesis and the compositions and densities of primary fluid inclusions in these minerals should agree with thermobarometric estimates from oxygen isotope thermometry and phase petrology. In fact, the inclusions are too poor in water and their density is too low to be compatible with the presumed X_{H_2O} of 0.46 of the peak metamorphic fluid and with the peak metamorphic conditions of 560–590 °C and 5.5-7.5 kbar. The isochores of CO_2–N_2±CH_4 inclusions in garnet plot well below the calculated peak metamorphic pressures and temperatures (Fig. 10). This discrepancy between independent thermobarometric estimates and the isochores of garnet- and kyanite-hosted fluid inclusions from the Radenthein complex does not necessarily exclude a primary origin of these inclusions. If these inclusions were indeed trapped during peak metamorphism, the observed fluid compositions and densities would merely indicate post entrapment modification. We consider two processes that may explain the observed phenomena: (1) selective water loss by diffusion and (2) chemical reactions between fluid and the host mineral.

As the interpretation of fluid inclusion textures may be ambiguous in medium to high grade metamorphic rocks, entrapment during retrograde stages must also be considered as a potential explanation for the low density, water-poor Type 2 inclusions. In the course of hydration reactions associated with retrogression, H_2O-free silicates (e.g. garnet and kyanite) are transformed to water-bearing ones (e.g. chlorite, muscovite). The remaining fluid becomes passively enriched in CO_2 and may eventually be trapped in fluid inclusions. In Radentheinite retrograde chlorite or muscovite is, however, rare, and removal of significant amounts of H_2O from a mixed-volatile peak metamorphic fluid by retrograde hydration reactions is very unlikely. Late transgranular fluid trails contain pure H_2O fluids and indicate the predominance of water in the late stage fluids, contradicting a retrograde origin of Type 2a and 2b CO_2-rich inclusions in garnet and kyanite.

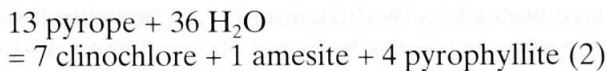Density reduction and flattening of the isochores in P-T space, which must be postulated for Type 2a inclusions in garnet, may indicate selective water loss by diffusion due to pressure and/or fugacity gradients between the inclusion and the external fluid (e.g. BAKKER and DIAMOND, 1998). At the presumed peak metamorphic conditions of 570 °C and 6.5 kbar the molar volume of a mixed CO_2–H_2O fluid with an X_{H_2O} of 0.46 is 31.4 cm³/mol. If in a hypothetical fluid inclusion with an initial molar volume of 31.4 cm³/mol and an X_{H_2O} of 0.46 all water is removed, then the molar volume of the remaining CO_2 fluid is increased to 58.1 cm³/mol. The corresponding isochore is shifted towards significantly lower pressures and it becomes flatter (Fig. 10). The new isochore plots below or at the lower pressure limit of the isochores, which were obtained from Type 2a inclusions. Selective water loss is a potentially very efficient mechanism to simultaneously lower the X_{H_2O} and increase the molar volume of an inclusion, and it may explain the high molar volumes observed in some Type 2a inclusions. However, essentially water-free Type 2a inclusions in garnet have molar volumes as low as 47 cm³/mol (see Table 5). This value is lower than would be expected from selective removal of water from the original peak metamorphic fluid by diffusion. This is why an alternative mechanism that allows for the selective removal of H_2O with a less pronounced or even opposite concomitant effect on the molar volume of the remaining fluid must be invoked.

Water may be selectively removed from a mixed-volatile fluid inclusion in the course of hydration reactions between the fluid and the host mineral. HEINRICH and GOTTSCHALK (1995) demonstrated that fluid-host mineral reactions may change fluid inclusion compositions and densities after entrapment. In order to test this hypothesis in the context of Type 2a inclusions, we modelled the P-T-X evolution of a hypothetical garnet-hosted H_2O–CO_2 inclusion, where chlorite is produced in the course of hydration of the garnet host. Here we briefly summarise the procedure. Details of the calculations are given in the Appendix.

As the molar volumes of garnet and chlorite are almost identical in the FeO–Al_2O_3–SiO_2–H_2O (FASH) and the MgO–Al_2O_3–SiO_2–H_2O (MASH)-systems; calculations can be restricted to the MASH-system. A closed system inclusion fluid – host mineral reaction producing chlorite at the expense of garnet in the MASH-system may be written as:

$$3 \text{ pyrope} + 8 \, H_2O \\ = 1 \text{ clinochlore} + 1 \text{ amesite} + 4 \text{ quartz} \quad (1)$$
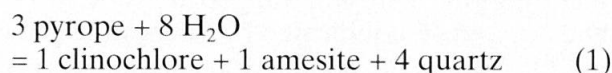
Another chlorite producing reaction may be written as:

13 pyrope + 36 H_2O
= 7 clinochlore + 1 amesite + 4 pyrophyllite (2)

Reactions (1) and (2) may proceed in sequence or parallel, giving rise to a product assemblage dominated by chlorite with variable but in any case minor amounts of quartz and/or pyrophyllite. Many more reactions of this kind could be written if other sheet silicates such as montmorillonites and kaolinite, which would thermodynamically be favoured at successively lower temperatures, were considered. Theoretically the thermodynamically most stable assemblages at successively lower temperatures could be calculated. At low temperatures the kinetics of mineral reactions may, however, become very sluggish and the applicability of such calculations is debatable. As the knowledge of the inclusion assemblage is rather limited – only chlorite could be unambiguously identified petrographically within Type 2a inclusions in garnet – we regard considerations about the very late stage mineral reactions as highly speculative and restrict the following discussion to the effects of reactions (1) and (2).

The fact that neither quartz nor pyrophyllite were identified within Type 2a inclusion does not necessarily exclude reactions (1) and/or (2). Quartz and/or pyrophyllite may well have been overlooked as they should only be present in minor amounts. The volume proportions of quartz or pyrophyllite in the reaction products are only about ~18 vol% of quartz within 82 vol% of chlorite in the case of reaction (1) and ~8 vol% of pyrophyllite within 92 vol% of chlorite in the case of reaction (2) (see Appendix). It is very difficult to unambiguously identify such small amounts of quartz and/or pyrophyllite within the chlorite-dominated solid-phase aggregates in Type 2a inclusions. The net effect of reactions (1) and (2) is to selectively remove water from a mixed-volatile fluid and to simultaneously reduce the space that is available for the remaining inclusion fluid, as in both reactions the volume change of solid phases is positive. We choose reaction (1) to discuss these effects quantitatively. The procedure is, however, general and easily adapted to other reactions between inclusion fluid and host mineral.

Above 1 kbar reaction (1) is almost pressure independent and it is shifted towards lower temperatures when H_2O is diluted (Fig. 10). The isochore which corresponds to a hypothetical peak metamorphic inclusion trapped at 570 °C, 6.5 kbar and X_{H_2O}=0.46 is indicated by a heavy dashed line in Fig. 10. On cooling, excluding inclusion reequilibration, the internal pressure of the inclusion must change along the path given by the isochore. If the fluid inside the inclusion reacts with the garnet host according to reaction (1), water and garnet are continuously consumed and chlorite and quartz are produced. The space available for the remaining fluid decreases because the volume of the produced chlorite and quartz is larger than the volume of the consumed garnet. Simultaneously, the fluid becomes successively enriched in CO_2. The net effect is a decrease of the water content and an increase of the bulk fluid molar volume from 31.4 to 39.8 cm^3/mol. The corresponding isochore is shown as a dotted heavy line in Fig. 10. This isochore plots above the P-T range of the isochores that were obtained from Type 2a CO_2–N_2–CH_4 inclusions in garnet (stippled field in Fig. 10). From this we infer that metamorphic hydration reactions may well explain the compositional difference between the supposed peak metamorphic fluid and Type 2a inclusions. But they cannot explain the decrease in fluid densities. The hypothesized post-entrapment modification of the garnet-hosted Type 2a fluid inclusions is best explained by a combination of (a) diffusive loss of H_2O due to pressure and/or fugacity gradients between the fluid inclusions and the pore fluid and (b) of selective removal of H_2O in the course of chlorite-producing hydration reactions between the inclusion fluid and the garnet host. It must be stated that the hydration of garnet is not necessarily the only source of chlorite within the inclusions. Chlorite was stable during peak metamorphism and the chlorite present in Type 2a inclusions may, at least in part, be regarded as accidentally trapped solid phase.

A similar process may be envisaged for post-entrapment modifications of the kyanite-hosted Type 2b inclusions. Similarly to the garnet-hosted Type 2a inclusions, their water contents and densities are lower than those of the presumed peak metamorphic fluid. Type 2b inclusions are also partially filled with solid phase aggregates (Fig. 5b). Sheet silicates could be qualitatively identified in cracks and in dark, clouded domains within kyanite on the SEM and by FTIR. However, hydrous silicates were so far not unambiguously identified *within* kyanite-hosted fluid inclusions, and hydration reactions between inclusion fluids and the kyanite host remain speculative. Garnet is regarded to be resistant against deformation and selective water loss by diffusion (TOURET, 1981; ELVEVOLD and ANDERSEN, 1993; WHITNEY, 1996; HERMS and SCHENK, 1998). Due to its better cleavage kyanite is expected to be more susceptible to diffusive water loss.

Several studies reported pre- and peak- metamorphic fluid inclusions hosted in garnet (e.g. SRIKANTAPPA et al., 1992; ELVEVOLD and ANDERSEN, 1993; ANDERSEN et al., 1993; HERMS and SCHENK,
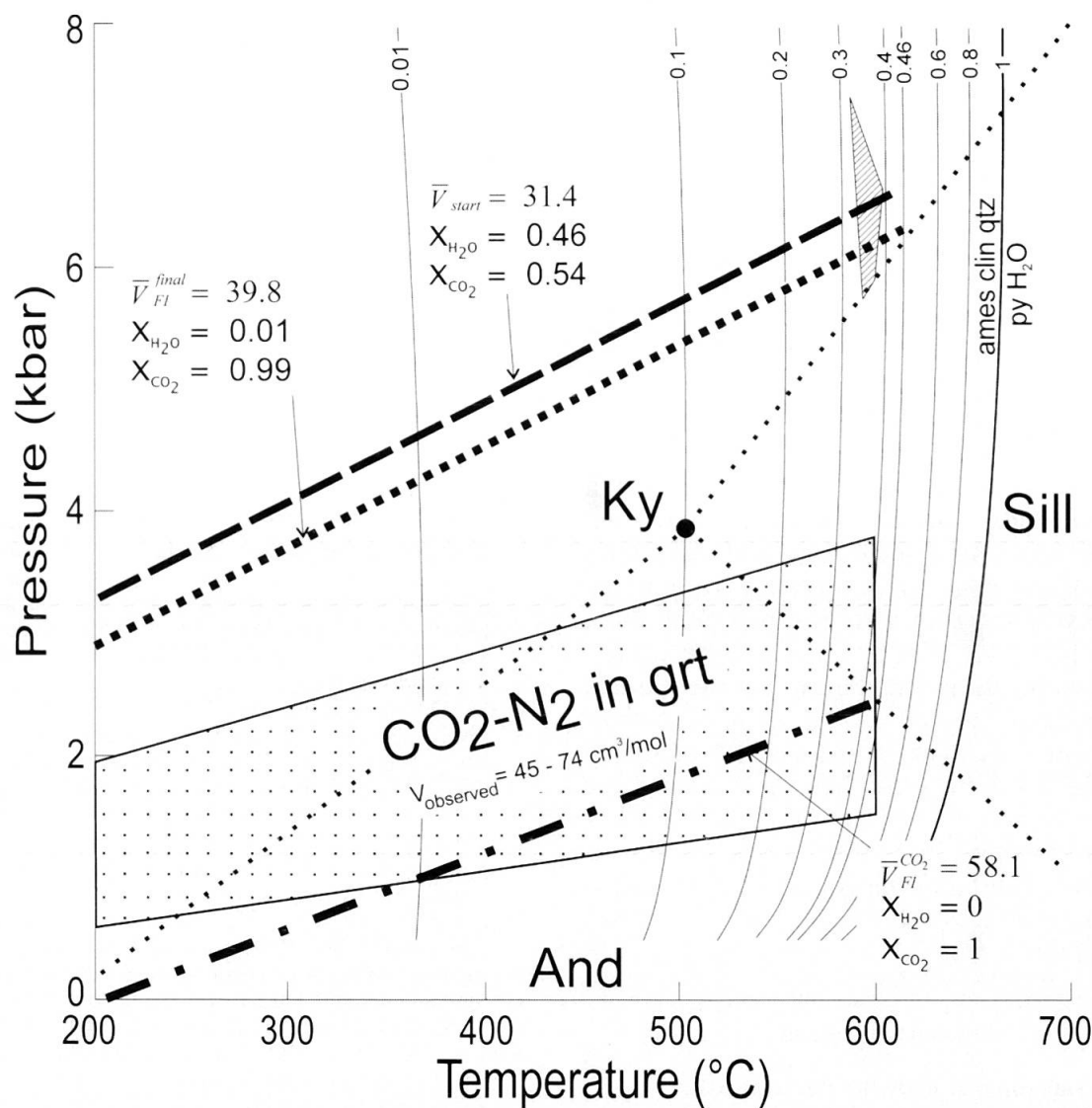
Fig. 10 Summary of microthermometry, thermobarometry and evolution of a hypothetical fluid inclusion. The isopleth for reaction (1) consuming garnet and H_2O and producing chlorite and quartz at $X_{H2O}=1$ is given by a subvertical heavy line in the right of the figure. The reaction shifts towards lower temperatures with decreasing water content of the fluid (light sub-vertical lines, numbers indicate X_{H2O}). The gray shaded field marks the peak metamorphic conditions of the Radentheinite as derived from independent methods. The stippled field indicates isochores calculated from microthermometry of Type 2a $CO_2-N_2\pm CH_4$ inclusions in garnet. The dashed heavy line represents the isochore of a hypothetical inclusion trapping a CO_2-H_2O fluid at 570 °C and 6.5 kbar with an X_{H2O} of 0.46. The dotted heavy line indicates the isochore of the same inclusion after consumption of the water component via production of chlorite and quartz at the expense of host garnet. The dash-dotted line represents the isochore of a hypothetical fluid inclusion that trapped the peak metamorphic fluid and lost its water content through selective diffusion of H_2O out of the inclusion. See text for further details.

1998; SCAMBELLURI et al., 1998; KAINDL et al., 1999) and in kyanite (PHILLIPOT et al., 1995; HAUZENBERGER et al., 1996; HÖLLER and HOINKES, 1996). Apart from textural criteria, the primary nature of these inclusions is usually inferred from the compatibility of the corresponding isochores with pressure-temperature estimates from independent methods. SRIKANTAPPA et al. (1992) argue that negative-crystal-shaped CO_2 inclusions in garnet from granulites of Southern India entrapped syn-peak-metamorphic pore fluids and have preserved original fluid densities and com-

positions. ELVEVOLD and ANDERSEN (1993) described vermicular CO_2-N_2 fluid inclusions in garnet from granulite-facies rocks of the Norwegian Caledonides, where the fluid densities were in excellent agreement with P-T-conditions deduced from geothermobarometry. In contrast, our example from the Radentein complex deduce that garnet- and kyanite-hosted fluid inclusions may suffer significant post-entrapment modification by both water loss through diffusion and chemical reactions between the inclusion fluid and the mineral host.

Conclusions

Out of several generations of garnet- and kyanite-hosted fluid inclusions from the Radenthein complex, high density nitrogen-bearing carbonic inclusions are interpreted as being of primary origin. Independent thermobarometric methods and phase petrology yield peak metamorphic conditions of 570 °C and 6.5 kbar and suggest the presence of a pore fluid with an X_{H_2O} of about 0.5. The fluid densities and water contents observed in the supposedly primary fluid inclusions are too low to be compatible with these conditions and post-entrapment modifications of the fluid inclusions must be invoked. Petrographic evidence such as the presence of chlorite aggregates in garnet-hosted primary fluid inclusions and theoretical considerations suggest that the water content and the density of the originally trapped peak metamorphic fluid were reduced by a combination of two processes. On the one hand, water loss by diffusion reduced the water content with a strong concomitant reduction of the density of the remaining fluid. On the other hand, water was selectively removed from the inclusions in the course of chlorite-forming hydration reactions between the inclusion fluid and the garnet host with no or only a minor effect on the bulk density of the remaining fluid.

References

ANDERSEN, T., AUSTRHEIM, H., BURKE, E.A.J. and SYNNOVE, E. (1993): N$_2$ and CO$_2$ in deep crustal fluids: evidence from the Caledonides of Norway. Chem. Geol. 108, 113–132.

ANDERKO, A. and PITZER, K.S. (1993): Equation-of-state representation of phase equilibria and volumetric properties of the system NaCl–H$_2$O above 573 K. Geochim. Cosmochim. Acta 57, 1657–1680.

AWERZGER, A. and ANGEL, F. (1948): Die Magnesitlagerstätte auf der Millstätter Alpe bei Radenthein (Kärnten). Radex-Rundschau 5, 91–95.

BAKKER, R.J. (1997): CLATHRATES: computer programs to calculate fluid inclusion V-X properties using clathrate melting temperatures. Comput. Geosci. 23, 1–18.

BAKKER, R.J. and DIAMOND, L.W. (1998): Reequilibration of synthetic CO$_2$–H$_2$O fluid inclusions in quartz. In: VANKO, D.A. and CLINE, J.S. (eds): PACROFI VII Conference Proceedings. Las Vegas, Nevada, 10.

BAKKER, R.J. (2001): Fluids: new software package to handel microthermometric data and to calculate isochores. In: NORONHA, F., DORIA, A. and GUEDES, A. (eds): ECROFI XVI, European Current Research on Fluid Inclusions, Abstracts. Universidade do Porto. Memória n° 7, 23–25.

BEBOUT, G.E. and FOGEL, M.L. (1992): Nitrogen-isotope compositions of metasedimentary rocks in the Catalina Schist, California: Implications for metamorphic devolatilization history. Geochim. Cosmochim. Acta 56, 2839–2849.

BOWERS, T.S. and HELGESON, H.C. (1983): Calculation of the thermodynamic and geochemical consequences of nonideal mixing in the system H$_2$O–CO$_2$–NaCl on phase relations in geologic systems: Equation of state for H$_2$O–CO$_2$–NaCl fluids at high pressures and temperatures. Geochim. Cosmochim. Acta 47, 1247–1275.

BROWN, P.E. and HAGEMANN, S.G. (1994): MacFlinCor: A computer program for fluid inclusion data reduction and manipulation. In: DE VIVO, B. and FREZZOTTI, M.L. (eds): Fluid inclusions in minerals: methods and applications. Virginia Tech. Blacksburg, 231–250.

CAVARRETTA, G. and TECCE, F. (1995): Flincs and Flincalc: PC programs for fluid inclusion calculations. Comput. Geosci. 21, 715–717.

COLE, D.R. and OHMOTO, H. (1986): Kinetics of isotope exchange at elevated temperatures and pressures. In: VALLEY, J.W., TAYLOR, H.P.Jr. and O'NEIL, J.R. (eds): Stable isotopes in high temperature geological processes. Reviews in Mineralogy 16, 41–90.

CONNOLLY, J.A.D. (1990): Multivariable phase-diagrams; an algorithm based on generalized thermodynamics. Am. J. Sci. 290, 666–718.

DUAN, Z.H., MOLLER, N., GREENBERG, J. and WEARE, J.H. (1992): The Prediction of Methane Solubility in Natural-Waters to High Ionic-Strength from O-Degrees-C to 250-Degrees-C and from 0 to 1600 Bar. Geochim. Cosmochim. Acta 56, 1451–1460.

EILER, J.M., VALLEY, J.W. and BAUMGARTNER, L.P. (1993): A new look at stable isotope thermometry. Geochim. Cosmochim. Acta 57, 1079–1091.

ELVEVOLD, S. and ANDERSEN, T. (1993): Fluid evolution during metamorphism at increasing pressure – carbonic bearing and nitrogen bearing fluid inclusions in granulites from Oksfjord, North Norwegian Caledonides. Contrib. Mineral. Petrol. 114, 236–246.

GOLDSTEIN, J.I., NEWBURY, D.E., ECHLIN, P., JOY, D.C., ROMIG Jr., A.D., LYMAN, C.E., FIORI, C. and LIFSHIN, E. (1992): Scanning Electron Microscopy and X-ray Microanalysis, 2nd ed. Plenum Press, 820 pp.

GRAMBLING, J.A. (1990): Internally-consistent geothermometry and H$_2$O barometry in metamorphic rocks – the example garnet-chlorite-quartz. Contrib. Mineral. Petrol. 105, 617–628.

HAUZENBERGER, C.A., HÖLLER, W. and HOINKES, G. (1996): Transition from eclogite to amphibolite-facies metamorphism in the Austroalpine Ulten Zone. Mineral. Petrol. 58, 111–130.

HEINRICH, W. and GOTTSCHALK, M. (1995): Metamorphic reactions between fluid inclusions and mineral hosts. I. Progress of the reaction calcite+quartz =wollastonite+CO$_2$ in natural wollastonite-hosted fluid inclusions. Contrib. Mineral. Petrol. 122, 51–61.

HERMS, P. and SCHENK, V. (1998): Fluid inclusions in high-pressure granulites of the Pan-African belt in Tanzania (Uluguru Mts): a record of prograde to retrograde fluid evolution. Contrib. Mineral. Petrol. 130, 200–212.

HOINKES, G., HÖLLER, F., RANTITSCH, G., DACHS, E., HÖCK, V., NEUBAUER, F. and SCHUSTER, R. (1999):

Alpine metamorphism of the Eastern Alps. Schweiz. Mineral. Petrogr. Mitt. 79, 155–181.

HOLLAND, T.J.B., BAKER, J.M. and POWELL, R. (1998): Mixing properties and activity-composition relationships of chlorites in the system MgO–FeO–Al_2O_3–SiO_2–H_2O. Eur. J. Mineral. 10, 395–406.

HOLLAND, T.J.B. and POWELL, R. (1990): An enlarged and updated internally consistent thermodynamic dataset with uncertainties and correlations: The system K_2O–Na_2O–CaO–MgO–MnO–FeO–Fe_2O_3–Al_2O_3–TiO_2–SiO_2–C–H_2–H_2O. J. Metamorphic Geol. 8, 89–124.

HÖLLER, W. and HOINKES, G. (1996): Fluid evolution during high-pressure partial melting in the Austroalpine Ulten Zone, Northern Italy. Mineral. Petrol. 58, 131–144.

HOLLISTER, L.S. (1990): Enrichment of CO_2 in fluid inclusions in quartz by removal of H_2O during crystal-plastic deformation. J. Struct. Geol. 12, 895–901.

JACOBSEN, R.T., STEWART, R.B. and JAHANGIRI, M. (1986): Thermodynamic properties of nitrogen from the freezing line to 2000 K at pressures to 1000 MPa. Journal of Physical and Chemical Reference Data 2, 735–909.

JOHNSON, E.L. and HOLLISTER, L.S. (1995): Syndeformational fluid trapping in quartz: determining the pressure-temperature conditions of deformation from fluid inclusions and the formation of pure CO_2 fluid inclusions during grain-boundary migration. J. Metamorphic Geol. 13, 239–249.

KAINDL, R., HOINKES, G., KNOLL, P. and ABART, R. (1999): Fluid inclusions related to Variscan and Alpine metamorphism in the Austroalpine Ötztal Basement, Eastern Alps. Mineral. Petrol. 65, 29–49.

KERKHOF A.M.v.d. (1988): The system CO_2–CH_4–N_2 in fluid inclusions: theoretical modelling and geological applications. Ph.D. thesis, Free University Amsterdam, 266 pp.

KERRICK, D.M. and JACOBS, G.K. (1981): A modified Redlich-Kwong equation for H_2O, CO_2 and H_2O–CO_2 mixtures at elevated pressures and temperatures. Am. J. Sci. 281, 735–767.

KERKHOF, A.M.v.d. and HEIN, U.F. (2001): Fluid inclusion petrography. Lithos 55, 27–47.

KNOLL, P., SINGER, R. and KIEFER, W. (1990): Improving spectroscopic techniques by a scanning multichannel method. Appl. Spectrosc. 44, 776–782.

KRANZ, R.L. (1983): Micro-cracks in rocks: a review. Tectonophysics 100, 449–480.

KRETZ, R. (1983): Symbols of rock forming minerals. Am. Mineral. 68, 277–279.

LEAKE, B.E. and many others (1997): Nomenclature of Amphiboles – Report of the Subcommittee on Amphiboles of the International-Mineralogical-Association, Commission on New Minerals and Mineral Names. Am. Mineral. 82, 1019–1037.

LEE, B.I. and KESLER, M.G. (1975): A generalized thermodynamic correlation based on three parameter corresponding states. American Institute of Chemical Engineering 21, 510–527.

MACDONALD, A.J. and SPOONER, E.T.C. (1981): Calibration of a Linkam TH 600 programmable heating-cooling stage for microthermometric examination of fluid inclusions. Econ. Geol. 76, 1248–1258.

METZGER, F.W., KELLY, W.C., NESBITT, B.E. and ESSENE, E.J. (1977): Scanning electron microscopy of daughter minerals in fluid inclusions. Econ. Geol. 72, 141–152.

PHILLIPOT, P., CHEVALLIER, P., CHOPIN, C. and DUBESSY, J. (1995): Fluid composition and evolution in coesite-bearing rocks (Dora-Maira massif, Western

Alps): implications for element recycling during subduction. Contrib. Mineral. Petrol. 121, 29–44.

RICHTER, R. and HOERNES, S. (1988): The application of the increment method in comparison with experimentally derived and calculated O-isotope fractionations. Chemie der Erde 48, 1–18.

ROEDDER, E. (1984): Fluid Inclusions. Reviews in Mineralogy 12, 644 pp.

SCAMBELLURI, M., PENNACHIONI, G. and PHILIPPOT, P. (1998): Salt-rich aqueous fluids formed during eclogitization of metabasites in the Alpine continental crust (Austroalpine Mt. Emilius unit, Italian western Alps). Lithos 43, 151–167.

SCHIMANA, R. (1986): Neue Ergebnisse zur Entwicklungsgeschichte des Kristallins rund um Radenthein (Kärnten, Österreich). Mitt. Ges. Geol. Bergbaustud. Österr. 33, 221–232.

SHARP, Z.D. (1990): In situ laser-microprobe techniques for stable isotope analysis. Chem. Geol. 101, 3–19.

SHARP, Z.D. (1995): Oxygen isotope geochemsitry of the Al_2SiO_5 polymorphs. Am. J. Sci. 295, 1058–1076.

SIMMONS, G. and RICHTER, D. (1976): Micro-cracks in rocks. In: STRENS, R.G.J. (ed.): The Physics and Chemistry of Minerals and Rocks. Wiley, New York, 105–137.

SRIKANTAPPA, C., RAITH, M. and TOURET, J.L.R. (1992): Synmetamorphic high-density carbonic fluids in the lower crust: Evidence from the Nilgiri Granulites, Southern India. J. Petrol. 33, 733–760.

THIERY, R., A.M.v.d. KERKHOF, A.M. and DUBESSY, J. (1994): vX properties of CH_4–CO_2 and CO_2–N_2 fluid inclusions: modelling for T<31 °C and P<400 bars. Eur. J. Mineral. 6, 753–771.

TOURET, J.L.R. (1981): Fluid inclusions in high-grade metamorphic rocks. In: HOLLISTER, L. and CRAWFORD, M.L. (eds): Short course in fluid inclusions: Applications to petrology. Mineralogical Association of Canada. Short Course Handbook 6, 182–208.

TOURET, J.L.R. (2001): Fluids in metamorphic rocks. Lithos 55, 1–25.

VITYK, M.O. and BODNAR, R.J. (1995): Do fluid inclusions in high-grade metamorphic terranes preserve peak metamorphic density during retrograde decompression? Am. Mineral. 80, 641–644.

VRY, J.K. and BROWN, P.E. (1991): Texturally-early fluid inclusions in garnets: evidence of the prograde metamorphic path? Contrib. Mineral. Petrol. 108, 271–282.

WEDEPOHL, K.H. (1978): Handbook of geochemistry. Springer, Berlin.

WHITNEY, D.L., MECHUM, T.A., DILEK, Y. and KUEHNER, S.M. (1996): Modification of garnet by fluid infiltration during regional metamorphism in garnet through silimanite-zone rocks, Dutchess County, New York. Am. Mineral. 81, 696–705.

YARDLEY, B.W.D. and SHMULOVICH, K.I. (1995): An introduction to crustal fluids. In: SHMULOVICH, K.I., YARDLEY, B.W.D. and GONCHAR, G.G. (eds): Fluids in the crust. Chapman & Hall, London, 1–10.

ZHENG, Y.-F. (1993): Calculation of oxygen isotope fractionation in hydroxyl-bearing silicates. Earth Planet. Sci. Lett. 120, 247–263.

Appendix

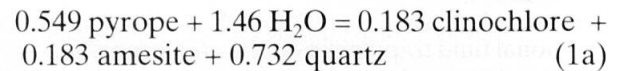Calculation procedure for a hypothetical fluid inclusion in garnet:

We calculated the equilibrium conditions for the reaction

$$3 \text{ pyrope} + 8 \text{ H}_2\text{O}$$
$$= 1 \text{ clinochlore} + 1 \text{ amesite} + 4 \text{ quartz} \qquad (1)$$
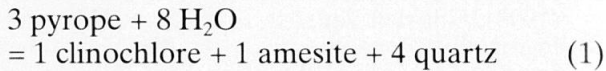
based on the thermodynamic data of HOLLAND and POWELL (1998) for various water contents starting at pure water ($X_{H_2O} = 1$) down to almost pure CO_2 ($X_{H_2O} = 0.01$; Fig. 10, Table 6). The X_{Mg} of the host garnet was taken from SEM analyses. As direct estimation of the Fe/Mg ratio of chlorite within inclusions was not possible, the X_{Mg} of chlorite was approximated using the Fe-Mg partitioning model of GRAMBLING (1990) for conditions of 570 °C and 6.5 kbar. The activity of pyrope was calculated assuming ideal mixing: Clinochlore and amesite activities were calculated after HOLLAND et al. (1998). The equation of state (EOS) of KERRICK and JACOBS (1981) and the software package FLUIDS by BAKKER (2001) were used for calculation of fluid molar volumes and isochores.

The calculation starts by assuming a hypothetical fluid inclusion trapped at T = 570 °C and P = 6.5 kbar, containing V_{Fl}^{start} = 100 cm³ H_2O–CO_2 fluid mixture of $X_{H_2O} = 0.46$. Inserting these data into a suitable EOS yields a fluid molar volume, which is equal to the bulk molar volume of the inclusion $\bar{V}_{start}$ = 31.4 cm³/mol. As the molar volume $\bar{V}$ is defined as $\bar{V} = V/n$, n = number of mol, there are $n_{Fl}^{total} = V/\bar{V} = 100/31.4 = 3.18$ mol H_2O–CO_2 fluid inside the inclusion. The number of mol H_2O and CO_2 are then $n_{H_2O} = n_{Fl}^{total} \times X_{H_2O} = 3.18 \times 0.46 = 1.46$ mol and $n_{CO_2} = n_{Fl}^{total} \times X_{CO_2} = 3.18 \times 0.54 = 1.72$ mol. In the hypothetical fluid inclusion a total of 1.46 mol of H_2O is available for the production of chlorite and quartz according to reaction (1). In reaction (1), 8 mol H_2O and 3 mol pyrope are necessary to produce 2 mol of chlorite and 4 mol of quartz. Defining a reaction progress parameter $p = n_{H_2O}/n_{H_2O}^{final} = 1.46/8 = 0.183$ and multiplying with each reaction coefficient, e.g. $n_{pyrope} = p \times n_{pyrope}^{total} = 0.183 \times 3 = 0.549$, reaction (1) reads as:

$$0.549 \text{ pyrope} + 1.46 \text{ H}_2\text{O} = 0.183 \text{ clinochlore} +$$
$$0.183 \text{ amesite} + 0.732 \text{ quartz} \qquad (1a)$$

The volume of e.g. consumed pyrope is $V_{pyrope} = n_{pyrope} \times \bar{V}_{pyrope} = 0.549 \times 113.15 = 62.16$ cm³ (HOLLAND and POWELL, 1990), for the volumes of the other phases involved see Table 6. The total volume of the hypothetical inclusion after consumption of 1.43 mol of H_2O is then $V_{Fl}^{final} = 100 + 62.16 - 38.62 - 38.42 - 16.62 = 68.50$ cm³. The bulk molar volume of this inclusion is $\bar{V}_{Fl}^{final} = V_{Fl}^{final}/n_{CO_2}^{final} = 68.5/1.72 = 39.8$ cm³/mol.